EAI Endorsed Transactions
on Industrial Networks and Intelligent Systems
Research Article EAI.EU

Intelligent Reflecting Surface assisted RF Energy Harvesting Mobile Edge Computing NOMA Networks: Performance Analysis and Optimization

Dac-Binh Ha[1,*], Van-Truong Truong[1], Yoonill Lee[2]

[1]Faculty of Electrical-Electronic Engineering, School of Engineering and Technology, Duy Tan University, Da Nang, 550000, Vietnam and the Institute of Research and Development, Duy Tan University, Da Nang, 550000, Vietnam.
[2]Faculty of Electrical Engineering Technology at the College of Lake County, Grayslake, IL, USA

Abstract

In this paper, we focus on the performance analysis and optimization of an RF energy harvesting (EH) mobile edge computing (MEC) network by the assistance of the intelligent reflecting surface (IRS) and non-orthogonal multiple access (NOMA) schemes. Specifically, a pair of users harvest RF energy from a hybrid access point (HAP) and offloads their tasks to the MEC server at HAP through wireless links by employing an IRS-aided and uplink NOMA scheme. To evaluate the performance of this proposed system, the closed-form expressions of successful computation and energy transfer efficiency probabilities are derived. We further formulate a multi-objective optimization problem and propose an algorithm to find the optimal energy harvesting time switching ratio value to achieve the best performance, namely SENSGA-II. Moreover, the impacts of the network parameters are provided to draw helpful insight into the system performance. Finally, the Monte-Carlo simulation results are shown to confirm the correctness of our analysis. The results have shown that the deployment of IRS can improve the performance of this considered RF EH NOMA system by increasing the number of reflecting elements.

Received on 08 June 2022; accepted on 09 August 2022; published on 11 August 2022

Keywords: mobile edge computing, intelligent reflecting surface, radio frequency energy harvesting, non-orthogonal multiple access, successful computation probability, energy consumption probability

doi:10.4108/eetinis.v9i32.1376

1. Introduction

In recent years, the Internet of Things (IoT) has been proliferating and applied in many different areas, e.g., industry, agriculture, transportation, military, and so on. Many latency-sensitive applications exist, such as virtual reality, autonomous driving, and interactive online gaming [1]. The mobile edge computing (MEC) approach has been proposed to support new applications and services that have significant data with latency constraints [2–4]. In the MEC paradigm, the servers with powerful computation ability move to the edge of the network to aid users in executing tasks via wireless links.

In fact, MEC has been proposed in many scenarios and has shown a positive impact when improving the performance of ultra-reliable and low latency communications (URLLC) systems [5, 6]. The authors in [5] recommend a digital twin metaverse based on MEC that guarantees real-time requirements. Specifically, industrial IoT devices are connected to the access point (AP) via the URLLC link and get the computation as well as caching supporting services to reduce system latency. An alternating optimization approach solves the latency optimization problem. The results show that the proposed optimization model and algorithm improve system performance. A case study on MEC is presented

*Corresponding author. Email: hadacbinh@duytan.edu.vn
This article was presented in part at the International Conference on Industrial Networks and Intelligent Systems (INISCOM), 2022.

in [6], which presents the design of a MEC system with task offloading and resource allocation requirements. Besides theoretical calculations, the authors also build an experimental model based on Intel's hardware, namely the EdgeFlow system. Experimental results show that the system can improve the computational efficiency from 15 to 45% compared to the local computing system.

However, many challenges are still posed when implementing IoT based on MEC systems in practice. Besides the limited computing capability of mobile edge devices, they are often equipped with energy-limited batteries to ensure dimensions standards. Accordingly, radio frequency (RF) power transfer is a new approach to supply energy for wireless devices based on RF waves [7, 8]. This solution is expected to prolong the life of network connections, extend coverage range, and improve communication network performance. RF power stations can be built independently of the MEC network as dedicated RF power stations, microwave stations, and TV towers [9]. In addition, RF power stations can also be integrated with access points called hybrid stations [10–12]. In [12], the authors investigate the MEC model applied in industrial IoT using RF energy harvesting (EH). In particular, two industrial sensor clusters operate according to the cluster head mechanism to collect radio energy from the hybrid AP to offload the tasks to the MEC server. Experiments of EH time, transmit power, task length, and the number of SNs in each cluster are analyzed to clarify the efficiency of the proposed MEC-based system.

Besides, billions of devices connected to IoT applications can create a complex operating scenario. It leads to orthogonal multiple access techniques such as FDMA and TDMA use of frequency or time resources which may not work inefficiency. The non-orthogonal multiple access (NOMA) approaches are considered a solution to improve spectrum efficiency, fair power distribution, and enhance network performance [13–16]. In [15], the authors investigated a two-user SISO NOMA MEC uplink model, which was supported by offloading to an AP. The simulation results show that incorporating the NOMA technique in the MEC network can significantly improve system performance compared to the traditional approach. For a more complex model, in [16], the authors studied a system model of a wireless sensor network with two groups of NOMA users and a multi-antenna access point, in which the best antenna and user selection scheme are used to enhance the performance of the NOMA MEC system.

In addition, to improve the performance of the wireless communication system, the intelligent reflecting surface (IRS) was proposed and attracted much research attention [17–19]. The IRS consists of a two-dimensional passive element array, where each element can independently create some change to the incident signal, e.g., the phase, amplitude, and frequency. IRS can be placed between transmitters and receivers, e.g., on a building wall, to create an intelligent communication environment. It is a cost-effective solution to enhance the performance of B5G and 6G wireless communication networks; thus, it has attracted increasing interest as a hot research topic [20–24]. For instance, the authors in [24] investigate the RIS-assisted communication downlink model for MIMO networks. Specifically, the base station communicates with users via RIS panels deployed in unmanned aerial vehicles (UAVs). The system is proven to deliver outstanding performance in terms of total network throughput and worst-case throughput of the users.

To the best of our knowledge, a few works focused on the combination of IRS and/or wireless power transfer and NOMA in MEC networks [25–27]. In [25], the NOMA and TDMA schemes of an IRS-aided two-NOMA-user MEC system are investigated to clarify the integration of IRS and NOMA in MEC networks. The results showed that NOMA is better than TDMA for the sum delay minimization when the users' cloud-computing time is sufficiently short. The integration of RF EH, IRS, and NOMA into MEC networks was studied in [26], where a hybrid access point provides RF energy and computing services to multiple NOMA users. Under the dynamic IRS beamforming framework for NOMA and TDMA schemes, computation rate maximization problems were formulated and solved by jointly optimizing the IRS passive BF and the resource allocation. A system model of a pair of near and far NOMA users and an IRS to assist the far user in offloading tasks is investigated in [27]. The performance analysis of this IRS-aided MEC network was studied by deriving the closed-form expression of successful computation probability.

In this work, we extend the work of [27], where the integration of RF EH, IRS, and NOMA is combined into the MEC system. Specifically, we consider the scenario where two users harvest energy from the hybrid access point (**HAP**) and offload their tasks to the server located at **HAP** with the assistance of an IRS. The main contributions of our paper are as follows:

- A quadra-phase protocol for RF EH IRS-aided mobile edge computing system based on the NOMA scheme is proposed.
- The considered system's closed-form expressions of successful computation and energy transfer efficiency probabilities are derived.
- The multi-objective optimization problem with two objective functions, i.e., successful computation probability and energy transfer efficiency probability, is formulated under the constraint of the time switching ratio. Accordingly, an algorithm

based on a genetic algorithm, namely SENSGA-II, is proposed to find the optimal front to achieve the best performance for this proposed system.

- The impact of network parameters, e.g., transmit power, time switching ratio, bandwidth, and task bit allocation, on the system performance is examined by numerical results to verify the efficiency and effectiveness of RF EH, IRS, and NOMA deployment in the MEC network.

The rest of this paper is organized as follows. Section II presents the proposed system model. The performance analysis and optimization of this considered system are provided in Section III. The numerical results and discussion are shown in Section IV. Finally, we draw a conclusion for our work in Section V.

2. System and Channel Model

We describe the notations used in the next part of this paper in Table 1.

TABLE 1. Notations

Notation	Meaning
m_i,m_H	Fading severity factor of Nakagami-m
δ	Path-loss exponent
$\mathbf{h_1} \in \mathbb{C}^{1\times 1}$	The small-scale fading vector of $\mathbf{U}_1 -$ **HAP** link
$\mathbf{h_2} \in \mathbb{C}^{N\times 1}$	The small-scale fading vector of $\mathbf{U}_2 -$ **IRS** links
$\mathbf{H} \in \mathbb{C}^{1\times N}$	The small-scale fading vector of **HAP** $-$ **IRS** links
N	Number of reflecting elements of IRS
P_0	Transmit power of **HAP**
γ_0	Average transmit SNR
η	Energy conversion efficiency
f	CPU-cycle frequency of **HAP**
ξ	The number of required CPU cycles for each bit of **HAP**
W	Channel bandwidth
L	The length of the task

We consider an RF EH IRS NOMA MEC system depicted in Fig. 1 and the time flowchart of this considered system is shown in Fig. 2.

Due to the real-time requirement and limited computation resources, a pair of energy-constrained users $\mathbf{U}_i$, $i \in \{1, 2\}$, cannot implement their tasks locally. Hence, they harvest RF energy from a hybrid access point (**HAP**) to offload the tasks to a MEC server located at **HAP**, which has outperformed the computation resource. There are blocking objects between users and **HAP** in many practical scenarios. The signal of users cannot reach **HAP** and vice versa.

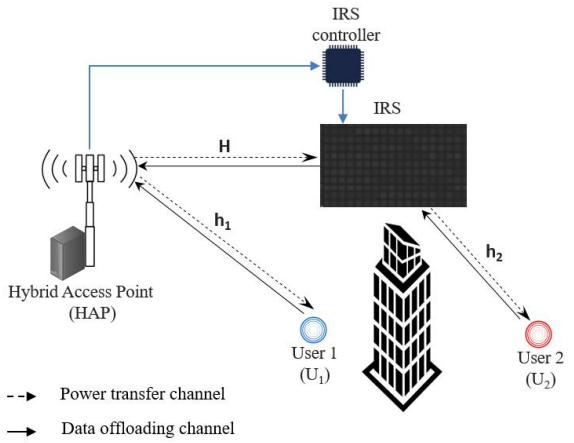

Figure 1. System Model for RF Energy Harvesting IRS-assisted MEC Network

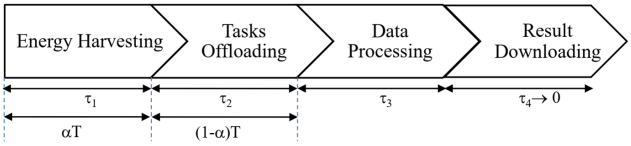

Figure 2. Time flowchart of the considered RF EH IRS-assisted MEC system

In this work, we assume that $\mathbf{U}_1$ is near to **HAP** without blocking objects. Meantime, $\mathbf{U}_2$ is far from **HAP** and there are blocking objects between $\mathbf{U}_2$ and $\mathbf{U}_1$ as well as $\mathbf{U}_2$ and **HAP**. Thus, an **IRS** consisting of N reflecting elements is deployed in the cell to assist $\mathbf{U}_2$'s transmission. Assuming that the element spacing of the IRS is high enough so that the small-scale fading associated with two different reflecting elements is independent. Moreover, all devices are assumed to have a single antenna and operate in the half-duplex mode. For the sake of simplicity, $\mathbf{U}_i$ is assumed to have a number of tasks with the same length of L_i bits for offloading.

We denote $\mathbf{H}$, $\mathbf{h_1}$, and $\mathbf{h_2}$ as the small-scale fading vectors of **HAP** $-$ **IRS**, **HAP** $-\ \mathbf{U_1}$, and $\mathbf{U}_2 -$ **IRS** links, respectively. More specifically, they are $\mathbf{H} = [g_{11}, g_{12}, ..., g_{1N}]$, $\mathbf{h_1} = [h_1]$ and $\mathbf{h_2} = [h_{21}, h_{22}, ..., h_{2N}]^T$, respectively. d_1, d_{21} and d_{22} denote the distances from **HAP** to $\mathbf{U}_1$, **HAP** to **IRS** and from $\mathbf{U}_2$ to **IRS**, respectively. $\alpha_1 \triangleq (d_1)^{-\delta}$, $\alpha_2 \triangleq (d_{21}d_{22})^{-\delta}$ stand for distance-based large-scale path loss where δ denotes the path loss exponent.

The transmission protocol of this considered system, namely an EH-IRS-MEC scheme, can be divided into four phases.

- Phase 1 (energy harvesting): **HAP** transfers the RF energy to $\mathbf{U}_i$ during the time of $\tau_1 = \alpha T$, where α denotes the time switching ratio, i.e., $0 < \alpha < 1$, and

T stands for transmission block time. Note that, **IRS** assists **HAP** in transferring RF energy to $\mathbf{U}_2$.

The harvested energy of $\mathbf{U}_1$ and $\mathbf{U}_2$ during the duration of αT are respectively written as

$$E_1 = \eta P_0 |h_1|^2 \alpha T, \tag{1}$$

$$E_2 = \eta P_0 |\mathbf{H\Phi h_2}|^2 \alpha T, \tag{2}$$

where $0 < \eta \leq 1$ stands for the energy conversion efficiency of the receiver [28], and P_0 denotes the transmit power of **HAP**.

- Phase 2 (task offloading): $\mathbf{U}_1$ and $\mathbf{U}_2$ an apply uplink NOMA scheme to offload their tasks to MEC server with the help of **IRS** during the time of (τ_2). The received signal of offloading tasks at **HAP** is expressed as

$$y = h_1 \sqrt{\alpha_1 P_{U_1}} s_1 + \mathbf{H\Phi h_2} \sqrt{\alpha_2 P_{U_2}} s_2 + w, \tag{3}$$

where P_{U_i} represents the transmit power of the i^{th} user, $i \in \{1, 2\}$; s_i denotes the offloading task of the i^{th} user, $i \in \{1, 2\}$; $w \sim \mathcal{CN}(0, \sigma^2)$ represents the AWGN at **HAP**. $\mathbf{\Phi} \triangleq \text{diag}\left[\beta_1 e^{j\theta_1}, \beta_2 e^{j\theta_2}, ..., \beta_N e^{j\theta_N}\right]$, where $j = \sqrt{-1}$, $\beta_n \in [0, 1]$ and $\theta_n \in [0, 2\pi)$, $n \in \{1, ..., N\}$, are the amplitude-reflection and phase-shift variable of the n^{th} element of IRS. The duration of Phase 2 is calculated as:

$$\tau_2 = \max_i \left\{ \frac{L_i}{W \log_2 (1 + \gamma_i)} \right\}, \tag{4}$$

where L_i and W_i stand for the task length and channel bandwidth with respect to $\mathbf{U}_i$, respectively. γ_i denotes the signal-to-interference-plus-noise ratio (SINR) and the signal-to-noise ratio (SNR) at **HAP** to decode s_i.

- Phase 3 (task executing): In this phase, the successive interference cancellation (SIC) is applied at **HAP** to mitigate the inter-user interference. At this time, **HAP** detects the signal s_i separately and decodes and computes the tasks of P_{U_i} during the time of τ_3. The duration of Phase 3 is given by:

$$\tau_3 = \frac{\xi L}{f}. \tag{5}$$

- Phase 4 (result downloading): At last, during the time of τ_4, **HAP** returns the computing results to users by applying the downlink NOMA scheme. In this work, we assume that τ_4 is very small compared to τ_1, τ_2 as well as τ_3 and thus is omitted (τ_4=0) [11, 15].

The transmit power of $\mathbf{U}_1$ and $\mathbf{U}_2$ are respectively given by

$$P_{U_1} = \frac{\eta P_0 |h_1|^2 \alpha T}{(1 - \alpha) T} = a P_0 X, \tag{6}$$

$$P_{U_2} = \frac{\eta P_0 |\mathbf{H\Phi h_2}|^2 \alpha T}{(1 - \alpha) T} = a P_0 Y, \tag{7}$$

where $a \triangleq \frac{\eta \alpha}{(1-\alpha)}$, $X \triangleq |h_1|^2$, $Y \triangleq |\mathbf{H\Phi h_2}|^2$.

By applying SIC, according to (3), the SINR and SNR at **HAP** to decode s_i are respectively obtained as follows:

$$\gamma_1 = \frac{a\gamma_0 \alpha_1 X^2}{a\gamma_0 \alpha_2 Y^2 + 1}, \tag{8}$$

$$\gamma_2 = a\gamma_0 \alpha_2 Y^2, \tag{9}$$

where $\gamma_0 \triangleq \frac{P_0}{\sigma^2}$ is the transmit SNR.

Note that, to improve the transmit environment, the parameters of IRS are reconfigured to obtain the best channel quality, i.e., to maximize $Z = |\mathbf{H\Phi h_2}| = |\sum_{n=1}^{N} \beta_n g_{1n} h_{2n} e^{j\theta_n}|$. It means that the phase-shift variables can be adjusted to obtain $Z_{\max} = \sum_{n=1}^{N} \beta_n |g_{1n}||h_{2n}|$. For the sake of simplicity, we assume $\beta_n = 1, \forall n$. Thus, according to [*Lemma*.2, [23]], the probability density function (PDF) and the cumulative density function (CDF) of $Z_{\max} = \sum_{n=1}^{N} |g_{1n}||h_{2n}|$ are expressed as

PDF:

$$f_Z(x) = \frac{m^N}{\Gamma(2m_s N)} x^{2m_s N - 1} e^{-2\sqrt{m_s m_l} x}, \tag{10}$$

CDF:

$$F_Z(x) = \frac{m^N (4m_s m_l)^{-m_s N}}{\Gamma(2m_s N)} \gamma\left(2m_s N, 2\sqrt{m_s m_l} x\right), \tag{11}$$

where $m_s = \min\{m_H, m_2\}$, $m_l = \max\{m_H, m_2\}$, $m = \frac{\sqrt{\pi} 4^{m_s - m_l + 1} (m_s m_l)^{m_s} \Gamma(2m_s) \Gamma(2m_l - 2m_s)}{\Gamma(m_s)\Gamma(m_l)\Gamma(m_l - m_s + \frac{1}{2})}$, m_H and m_2 denote the Nakagami-m fading parameters; $\gamma(.,.)$ is the lower incomplete gamma function.

3. Performance Analysis and Optimization

This section describes the performance analysis of this proposed system in terms of the successful computation and energy consumption probabilities. Furthermore, we formulate the optimization problem and propose the solution to solve this.

3.1. Performance analysis

We describe the performance analysis of this proposed IRS-aided MEC system in terms of successful computation probability and energy consumption probability.

The successful computation probability ($\mathbf{\Phi_s}$) is an important measure that is useful for system designers to evaluate the latency performance of the MEC networks [15]. $\mathbf{\Phi_s}$ is defined as the probability that all tasks are successfully executed within a required time T_{th}. For this proposed system, $\mathbf{\Phi_s}$ is expressed as

$$\mathbf{\Phi_s} = \Pr\left(\tau_1 + \tau_2 + \tau_3 + \tau_4 \leq T_{th}\right). \tag{12}$$

Due to $\tau_1 = \alpha T = \alpha(T_{th} - \tau_3)$, $\mathbf{\Phi_s}$ can be rewritten as

$$\mathbf{\Phi_s} = \Pr\left[\tau_2 \leq (1-\alpha)T\right], \tag{13}$$

where $T = T_{th} - \frac{\xi L}{f}$.

To evaluate the latency performance of this proposed RF EH IRS-assisted MEC system with NOMA scheme, the **Lemma 1** is derived as follows:

Lemma 1. In this considered RF EH IRS-aided MEC NOMA system, the closed-form expression of the successful computation probability $\mathbf{\Phi_s}$ is given by

$$\begin{aligned}\mathbf{\Phi_s} \approx\ & \frac{\pi a_0 m^N}{2Q_1\Gamma(2m_sN)} \sum_{k=0}^{m_1-1}\sum_{q=1}^{Q_1} \frac{m_1^k}{k!\lambda_1^k}(-\ln t_q)^{2m_sN-1} \\ & \times \left[b_1(-\ln t_q)^4 + b_2\right]^{\frac{k}{2}} e^{-\frac{m_1}{\lambda_1}\sqrt{b_1(-\ln t_q)^4+b_2}} \\ & \times \frac{e^{-2\sqrt{m_s m_l}(-\ln t_q)}}{t_q}\sqrt{1-x_q^2},\end{aligned} \tag{14}$$

where $a_0 = e^{-\sqrt[4]{b_0}}$, $b_0 = \frac{\gamma_2^{th}}{a(1-\rho)\alpha_2\gamma_0}$, $b_1 = \frac{\gamma_1^{th}(1-\rho)\alpha_2}{\rho\alpha_1}$, $b_2 = \frac{\gamma_1^{th}}{a\rho\gamma_0\alpha_1}$, $\gamma_1^{th} = 2^{\frac{L_1}{WT^*}} - 1$, $\gamma_2^{th} = 2^{\frac{L_2}{WT^*}} - 1$, $T^* = (1-\alpha)\left[T_{th} - \frac{\xi L}{f}\right]$, $L = L_1 + L_2$, $x_q = \cos\left(\frac{2q-1}{2Q_1}\pi\right)$, $t_q = \frac{(x_q+1)a_0}{2}$, Q_1 is the complexity-vs-accuracy trade-off coefficient.

Proof. See in Appendix A.

Moreover, the energy transfer efficiency is also an important performance metric that is used to characterize how much energy is actually transferred to offload in RF EH MEC networks.

Definition 1. The energy transfer efficiency (EFE) is defined as the ratio of instantaneous transferred energy to the corresponding instantaneous total offloading rate.

For this proposed system, EFE is given by

$$\mu_e = \frac{E_{trans}}{R_{total}}, \tag{15}$$

where $E_{trans} = P_0\alpha T$, $R_{total} = \sum_{i=1}^{2}(1-\alpha)W\log_2(1+\gamma_i)$, $i \in \{1,2\}$.

Remark 1. In contrast to common energy efficiency defined in existing works [29, 30], we define the EFE from the instantaneous perspective to show the transferred energy and instantaneous data rate simultaneously. Obviously, μ_e is a random value. Thus we consider its statistical property.

Definition 2. The energy transfer efficiency probability (EEP), denoted by $\mathbf{\Psi_e}$, is defined as the probability that the energy transfer efficiency falls below a predetermined threshold ψ_{th}.

For this proposed system, $\mathbf{\Psi_e}$ is expressed as

$$\mathbf{\Psi_e} = \Pr\left(\mu_e < \psi_{th}\right). \tag{16}$$

To evaluate the energy performance of this proposed RF EH IRS-aided MEC system, we derive the following **Lemma 2** as follows:

Lemma 2. In this proposed RF EH IRS-aided MEC NOMA system, the closed-form expression of the energy transfer efficiency probability $\mathbf{\Psi_e}$ is expressed as

$$\begin{aligned}\mathbf{\Psi_e} \approx\ & 1 - F_Z(a_1) + \frac{\pi a_1 m^N}{2Q_2\Gamma(2m_sN)} \sum_{k=0}^{m_1-1}\sum_{q=1}^{Q_2} \frac{m_1^k}{k!\lambda_1^k} \\ & \times u_q^{2m_sN-1}\left[c_1 - c_2u_q^4\right]^{\frac{k}{2}} e^{-\frac{m_1}{\lambda_1}\sqrt{c_1-c_2u_q^4}-2\sqrt{m_sm_l}u_q} \\ & \times\sqrt{1-x_q^2},\end{aligned} \tag{17}$$

where $\gamma_{th} = 2^{\frac{\alpha T P_0}{(1-\alpha)W\psi_{th}}}$, $c_1 = \frac{\gamma_{th}-1}{a\gamma_0\alpha_1}$, $c_2 = \frac{\alpha_2}{\alpha_1}$, $a_1 = \sqrt[4]{\frac{c_1}{c_2}}$, $x_q = \cos\left(\frac{2q-1}{2Q_2}\pi\right)$, $u_q = \frac{(x_q+1)a_1}{2}$, Q_2 is the complexity-vs-accuracy trade-off coefficient.

Proof. See in Appendix B.

3.2. Optimization: Problem formulation and solution

We are interested in the design optimization problem to jointly optimize the SCP and EEP for the RF EH IRS-aided NOMA MEC system as follows:

$$(\text{P1}): \max_{\alpha}\ (\Phi_s, \Psi_e) \tag{18a}$$

$$\text{subject to:}\quad 0 \leq \alpha \leq 1 \tag{18b}$$

where (P1) belongs to the class of multi-objective optimization problems, here specifically, maximizing SCP and EEP. Constraint (18b) describes the condition of the time allocation factor of the users. From the performance definitions of the proposed system, it is easy to see that SCP and EEP are two correlated objective functions; i.e., maximizing SCP could negatively result in EEP maximization; and vice versa. Therefore, the optimal outcome (P1) is not unique but a set of optimal results, representing the best correlation between SCP and EEP. For single-objective optimization, the fitness values (FV) of objective function always have complete order because when considering any two FVs; namely Ω_1 and Ω_2, there always exist two cases are $\Omega_1 < \Omega_2$ or $\Omega_1 \geq \Omega_2$. However, for the problem (P1), we need to use the dominant concept to compare the FVs, as follow

Definition 3. A feasible solution α_1 dominates over the solution α_2 with $\alpha_1 \neq \alpha_2$, denoted by $\alpha_1 \preceq \alpha_2$, if and only if,

$$\begin{cases}\Phi_s(\alpha_1) \leq \Phi_s(\alpha_2) \\ \Psi_e(\alpha_1) \leq \Psi_e(\alpha_2) \\ \Phi_s(\alpha_1) < \Phi_s(\alpha_2) || \Psi_e(\alpha_1) > \Psi_e(\alpha_2)\end{cases}, \tag{19}$$

In this study, we use the Pareto curve to represent the optimal group of results (P1) [31]. A solution is the Pareto optimal if any others do not outperform it in the objective space. The set of possible solutions that are not dominated is called the Pareto optimal set, and their corresponding FVs are called Pareto Front (PF). Accordingly, we transform the objective functions so that (P1) can be expressed by PF. Specifically, the compensation functions of SCP and EEP, i.e., $\overline{\Phi_s} = 1 - \Phi_s$, $\overline{\Psi_e} = 1 - \Psi_e$, will be used as the objective function, and the problem is transformed into determining the PF of the minimum functions. Thus, the proposed multi-objective optimization problem is rewritten as follows:

$$(\text{P2}) : \min_{\alpha} \left(\overline{\Phi_s}, \overline{\Psi_e}\right) \tag{20a}$$

$$\text{subject to:} \quad 0 \leq \alpha \leq 1 \tag{20b}$$

We propose to use the Non-dominated Sorting Genetic Algorithm II (NSGA-II) to determine the PF [32] for (P2), namely SENSGA-II. The SENSGA-II is a stochastic evolutionary multi-objective algorithm constructed based on combining two algorithms: genetic algorithm (GA) [33] to select and develop optimal individuals and crowding distance algorithm to get a reasonable distribution of optimal points on the PF [34]. Basic GA genetics concepts and operations, including crossover, mutation, and natural selection, are also used. The difference between the multi-objective and single-objective GA algorithms is in the fitness assignment, and how to maintain the elite population. The detailed presentation of SENSGA-II algorithm is given in **Algorithm 1**, specifically as follows:

- **Step 1:** Randomly initialize n_{Pop} individuals $p_i, (i = 1, ..., n_{Pop})$ for the population $\mathbb{P}$, where each element contains a gene that is also a solution of (P2) and satisfies (18b), i.e., α. Thus, in the t^{th} generation, the population is described by the formula:

$$\mathbb{P}(t) = (\alpha_1(t), \alpha_2(t), ..., \alpha_{n_{Pop}}(t)), \tag{21}$$

- **Step 2:** Calculate the fitness value of the objective functions that need to be optimized simultaneously, i.e., SCP and EEP, for $\mathbb{P}(t)$.

- **Step 3:** Call the Non-dominated Sorting (NdS) procedure, which uses (19) to determine the ranking of the input $\mathbb{P}(t)$. NdS assigns a first rank, namely $\mathcal{F}(1)$, to individuals that are not dominant in the population and excludes them from consideration. Then find a new set of non-dominated individuals to assign a second rank and so on until all individuals p_i are checked, $p_i \in \mathbb{P}(t)$. Thus, the output of NdS is a set of individuals sorted by ranking, namely $\mathcal{F}(k)$, where k is the index of ranking. Details of NdS steps are given in **Algorithm 2**.

- **Step 4:** Call the Crowding distance calculator (CDC) procedure with the input $\mathcal{F}(k)$. This step aims to find the sum of Euclidean distances from each individual to two neighboring solutions in each front based on two objective functions. Thereby, CDC estimates the density of solutions surrounding the solution under consideration, as follows:

$$\mathcal{CD}_{p_i} = \sum_{\Omega \in \{\Phi_s, \Psi_e\}} \frac{\Omega(p_{i+1}) - \Omega(p_{i-1})}{\Omega_{max} - \Omega_{min}}, \tag{22}$$

where $\mathcal{CD}_{p_i}$ is the crowding distance of p_i, Ω_{max} and Ω_{min} are the maximum and minimum of the fitness values, respectively, when using the objective function $\Omega, \Omega \in \{\Phi_s, \Psi_e\}$. Details of CDC steps are given in **Algorithm 3**.

- **Step 5:** The parent is selected based on their rank and crowding distance as follows: randomly select two solutions; if they have the same non-domination rank $\mathcal{F}(k)$, the solution which has $\mathcal{CD}_{p_i}$ higher will be chosen; otherwise, the solution with the lower rank will be selected. All selected parents are added to the matching pool to prepare for the crossover process.

- **Step 6:** Arithmetical crossovers [35] were used in this study to crossbreed the parent p_i and p_j. Let ζ_c be the crossover percentage. Two offspring individuals are given by the formula:

$$\begin{aligned} p_{h1}(t+1) &\leftarrow \delta_c p_i + (1 - \delta_c) p_j, \\ p_{h2}(t+1) &\leftarrow \delta_c p_j + (1 - \delta_c) p_i, \end{aligned} \tag{23}$$

where δ_c is an uniform arithmetical crossover factor, that is randomly chosen from 0 to 1.

- **Step 7:** In this step, non-uniform mutation, as (24), is applied such that the probability approaches zero as the number of evolution rounds increases. It makes the mutation operator efficient in the early stages of the algorithm, having a more negligible effect on the population as it evolves into the late stages.

$$\begin{cases} p_m(t) \leftarrow p_m(t) + (\alpha_{max} - p_m(t))\Delta, \tau = 0 \\ p_m(t) \leftarrow p_m(t) - (p_m(t) - \alpha_{min})\Delta, \tau = 1 \end{cases} \tag{24}$$

where $\Delta = 1 - r^{(1 - \frac{t}{MaxIt})^{\delta_b}}$, r is randomly chosen from 0 to 1, δ_b is selected following the level of dependency on the maximum number of iterations, τ is the random number that may have zero or one. Let ζ_m be the crossover percentage. Let the set of offspring based on the GA process be $\mathbb{Q}(t)$.

- **Step 8:** The NdS and CDC procedures are called to evaluate the elite-preservation population, denoted $\mathbb{O}$, which is the combination set of $\mathbb{P}(t-1)$ and $\mathbb{Q}(t)$, i.e., $\mathbb{O}(t) = \mathbb{P}(t-1) \cup \mathbb{Q}(t)$.

- **Step 9:** Select n_{Pop} elite individuals based on $\mathcal{F}(k)$ and $\mathcal{CD}_{p_i}$ which hold in **Step 8**. If the number of individuals belong to $\mathcal{F}(1)$ is less than n_{Pop}, the entire $\mathcal{F}(1)$ will be selected into $\mathbb{P}(t+1)$. The rest will be taken from the $\mathcal{F}(k)$, until enough n_{Pop} individuals. The set of p_i belong to $\mathcal{F}(1)$ is stored in PF. This process continues until the end of evolution.

Algorithm 1 SCP and EEP maximization based on NSGA-II (SENSGA-II)

Input: $\Phi_s, \Psi_e, n_{Pop}, MaxIt$
Output: PF
Initialize: $t \leftarrow 0, \mathbb{P}(0)$
Evaluate $\mathbb{P}(0)$ using (14) and (17)
Call: Non-dominated Sorting procedure (NdS) with $\mathbb{P}(0)$
Call: Crowding distance calculator procedure (CDC) with $\mathbb{P}(0)$
while $t \leq MaxIt$ **do**
    $t \leftarrow t+1$
    Choose $\mathbb{Q}(t)$ following ranking $\mathcal{F}(k)$ and crowding distance $\mathcal{CD}_{p_i}$ of $p_i \in \mathbb{P}(t-1)$
    Crossover for $\mathbb{Q}(t)$ using (23)
    Mutation for $\mathbb{Q}(t)$ using (24)
    $\mathbb{O}(t) = \mathbb{P}(t-1) \cup \mathbb{Q}(t)$
    Call: NdS with $\mathbb{O}(t)$
    Call: CDC with $\mathbb{O}(t)$
    Updated $\mathbb{P}(t)$
    Store PF
end while
Return PF

We further investigate the algorithm complexity of SENSGA-II as follows: In **Algorithm 2**, we perform rankings for $2n_{Pop}$ instances belonging to $\mathbb{O}(t)$ with two nested loops. In each loop, we evaluate two objective functions $\overline{\Phi_s}$ and $\overline{\Psi_e}$ with algorithmic complexity of $m_1 Q_1$ and $m_1 Q_2$, respectively. Thus, the total number of operations required for this procedure is:

$$\Upsilon_1 = m_1(Q_1 + Q_2)(2n_{Pop})^2. \tag{25}$$

For **Algorithm 3**, the sorting and comparison algorithm is applied to 2_{nPop} instances with two objective functions, so the total number of operations required for this procedure is as follows:

$$\Upsilon_2 = m_1(Q_1 + Q_2)(2n_{Pop}) \log(2n_{Pop}). \tag{26}$$

Algorithm 2 Non-dominated Sorting procedure (NdS)

Input: $\mathbb{P}(x)$
Output: $\mathcal{F}(k)$
Init $k = 1$ is the ranking index
$\mathcal{F}(k) = \emptyset$
for $p_i \in \mathbb{P}(x) \setminus \mathcal{F}(k)$ **do**
    Init $nonD_p = \emptyset$ is the set containing all the individuals that are not dominant than p_i
    Init $D_p = 0$ is the number of individuals that dominated p_i
    for $p_j \in \{\mathbb{P}(x) \setminus \mathcal{F}(k), p_i\}$ **do**
        if $p_i \preceq p_j$ **then**
            $nonD_p = nonD_p \cup p_j$
        else
            $D_p = D_p + 1$
        end if
        if $D_p == 0$ **then**
            $\mathcal{F}(k) = \mathcal{F}(k) \cup p_i$
        end if
        $k = k + 1$
    end for
end for
Return $\mathcal{F}(k)$

Algorithm 3 Crowding distance calculator procedure (CDC)

Input: $\mathcal{F}(k)$
Output: $\mathcal{CD}_{p_i}$
Assign n is the number of individuals in $\mathcal{F}(k)$
for $i = 2 : (n-1)$ **do**
    Init $\mathcal{CD}_{p_i} = 0$
    Init $\mathcal{CD}_{p_1} = \mathcal{CD}_{p_n} = \infty$
    Calculate $\mathcal{CD}_{p_i}$ using (22)
end for
Return $\mathcal{CD}_{p_i}$

Finally, the elite individual n_{Pop} natural selection operation has a complexity of:

$$\Upsilon_3 = (2n_{Pop}) \log(2n_{Pop}). \tag{27}$$

The overall complexity of the SENSGA-II algorithm is:

$$\mathcal{O}(\Upsilon_1 + \Upsilon_2 + \Upsilon_3) = \mathcal{O}(m_1(Q_1 + Q_2)(2n_{Pop})^2). \tag{28}$$

To evaluate the convergence of SENSGA-II, we use the diversity metric [32], denoted by $\mathcal{D}$, which measures the extent of spread achieved among the obtained solutions. The lower $\mathcal{D}$, the better convergence of the algorithm.

$$\mathcal{D} = \frac{(D_{e1} + D_{e2} + \sum_{i=1}^{n} |D_i - \overline{D}|}{D_{e1} + D_{e2} + (n-1)\overline{D}} \tag{29}$$

where D_{e1} and D_{e2} are the Euclidean distances from the extreme solutions to the neighboring solutions, respectively, for the two objective functions, $\overline{D}$ is the average Euclidean distance of PF.

4. Numerical Results and Discussion

This section analyzes the system behaviors in terms of SCP and EEP in the uplink RF EH IRS-aided NOMA MEC system. Furthermore, the simulation results are also provided to verify analytical results. Unless otherwise defined, the investigation parameters configuration is depicted in TABLE 2 [36].

TABLE 2. Simulation Parameters

Parameters	Notation	Typical Values
Environment		Nakagami-m
Fading parameters	m_{H_1},m_{h_1}, m_{H_2},m_{h_2}	3.0, 2.5, 2.5, 1.5
Distances	d_1,d_{21},d_{22}	10, 30, 20
Energy conversion coefficient	η	0.75
Number of IRS elements	N	1, 3, 10
Transmit SNR	γ_0	10-40 dB
Path-loss exponents	δ	2, 2.5
CPU-cycle frequency of **HAP**	f	1 GHz
The number of CPU cycles/bit	ξ	2
Channel bandwidth	W	1 MHz
The threshold of latency	T_{th}	0.01 s
The threshold of energy consumption	ψ_{th}	3 uJ
Number of points for Gaussian-Chebyshev quadrature method	P, Q	50
The maximum number of iterations	$MaxIt$	300
The population size	n_{Pop}	100
The crossover percentage	ζ_c	0.9
The mutation percentage	ζ_m	0.002

4.1. Impacts of average transmit SNR and the number of IRS elements

The impact of average transmit SNR (γ_0) and the number of IRS elements (N) on the performance of the plotted system is shown in Fig. 3. The solid lines are curves describing the SCP, while the dashed lines represent the EEP of the system. We find that the analyzes of SCP and EEP are accurate as all simulation results coincide with the corresponding analytical results derived from (16) and (17). The first observation that can be drawn is that all three curves describing the system's SCP have the same form as increasing as γ_0 increases. In other words, system performance improves when γ_0 has an excellent value. It is evident that because γ_0 increases, the user is supported more in terms of energy and improves the efficiency of the offloading process.

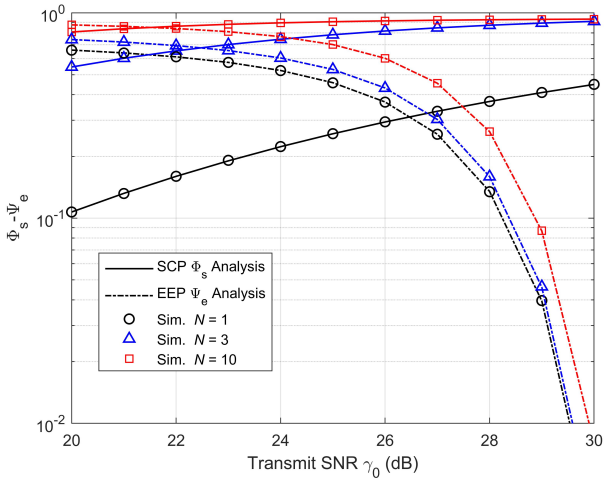

Figure 3. Impacts of average transmit SNR and the number of IRS elements

Nevertheless, when γ_0 gets too high, i.e., γ_0 exceeds 30 dB, the SCP tends to saturate.

Meanwhile, EEP tends to be the opposite of SCP, i.e., as γ_0 increases, EEP decreases. The reason is that EEP represents energy efficiency used, smaller EEP means high energy consumption, and conversely, large EEP means good energy efficiency. It is explained as follows: as γ_0 increases, that is, the transmit power at the HAP increases, and the energy used during offloading also increases, resulting in reduced energy efficiency gradually. Therefore, the trade-off between SCP and EEP is a concern when designing the proposed system. The transmit power parameters from the HAP need to be considered to ensure optimal SCP while keeping the EEP at an appropriate value. It also highlights the necessity of deploying multi-objective optimization algorithms for the proposed RF EH IRS-assisted NOMA MEC system.

Another observation mentioned is the significant dependence of SCP and EEP on N. Furthermore, as expected, as N increases, both SCP and EEP improve. The reason arises from two aspects. First, when increasing N, the different signal paths from HAP towards U_2 are added to the system, thus improving channel rank and spatial multiplexing gain. Second, the larger N is, the more energy can be collected by U_2 in the EH phase, resulting in enough power to use during the offloading phase, contributing to the elevation of the system's SCP. Furthermore, IRS reflectors can support U_2 energy collection without any transmit RF chains, so EEP will be significantly improved.

4.2. Impacts of the time switching ratio

The effect of the time switching ratio (α) on SCP and EEP is depicted in Fig. 4. We focused on observing the lines describing the SCP with the values γ_0 being

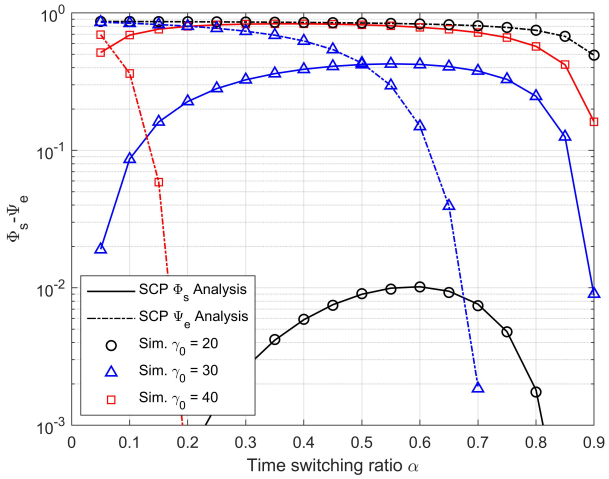

Figure 4. Impacts of the time switching ratio

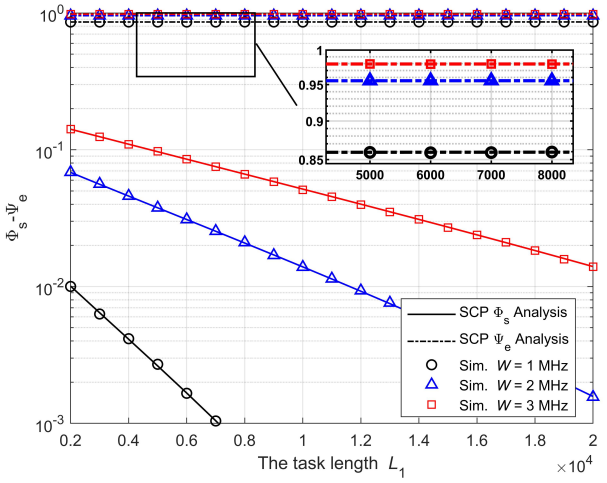

Figure 5. Impacts of the task length and the bandwidth

20 dB, 30 dB, and 40 dB, respectively. The obtained results show that SCP is a unimodal function according to the parameter α, i.e., SCP has only one maximum in the range α in $[0, 1]$. Thus, it is necessary to use the optimal algorithm to find α^* such that SCP reaches its maximum value. The dependence on α is evident because the SCP difference when α changes are substantial: when α is slight, i.e., $0 < \alpha < 0.2$ or when α approaches 1, the system's SCP is very low. It means that the system has a high probability of not completing tasks within the maximum allowable delay time. Equations (1) and (2) explain this: when α is too low, the energy collected by the user is not enough for them to perform offloading, resulting in low SCP. Meanwhile, when α is high, the time to offload and compute decreases, and the system does not have enough time to reach the offloading target, i.e., low SCP. In contrast, the system obtains high SCP with an adequately designed α coefficient. Another observation, the trend in EEP in Fig.4 shows low energy efficiency as α increases. According to (6) and (7), an increase in α leads to a rise in the user's transmit power, resulting in a decrease in EEP.

4.3. Impacts of the length of task and the bandwidth

Fig. 5 describes the effect of task length (L_1) on SCP and EEP in three different bandwidth scenarios, W = 1 MHz, W = 2MHz, and W = 3 MHz. The system's SCP decreases as the task sequence length increases. It is consistent with formula (4) because the task sequence length is proportional to the offloading time tau_2. Furthermore, as L_1 increases, the total number of bits that the HAP needs to process also increases, resulting in an increase in the computation time of tau_3 in phase 3. In short, the larger the offload bit sequence, the more budget time is required for offloading and processing, resulting in SCP degradation. The impact is enormous when the system's bandwidth is low. Observing the curve describing SCP when W = 1 MHz, we see its slope is steep: L increases from 2 kB to 7 kB, then SCP decreases up to 10 times. Continuing to compare with the SCP signal in the other two cases, we conclude that the larger the bandwidth, the better the SCP of the system. Furthermore, increasing bandwidth also positively affects EEP: i.e., as W increases, so does EEP, meaning increased energy efficiency. Therefore, bandwidth is a parameter that needs special attention when designing the RF EH IRS NOMA MEC system in practice.

More interestingly, the system EEP descriptor curve does not change with the change of task sequence length, and this trend is consistent for all three cases of bandwidth change. It can be explained by formula (17) when EEP is an independent function of the variable L_1. In terms of physical significance, we only consider EFE in terms of energy dissipated during transmission and investigate its statistical characteristics. Accordingly, EEP is expressed independently of the constraint in terms of maximum system latency, which depends on task sequence length as observed in SCP lines. Thus, in terms of the EEP perspective, the system is only required to meet the given energy threshold, regardless of the transmission rate. In simpler terms, the system can operate in a way that transmits bits at a slow data rate while holding the EFE condition, thereby allowing the desired EEP to be achieved.

4.4. Optimal algorithm experiments

Fig. 6 shows the non-dominated solutions obtained after 200 generations with SENSGA-II, with the average transmit power being 30 dB. We extract three solutions, A(0.8813, 0.521), B(0.9276, 0.3755), and C(0.9984,

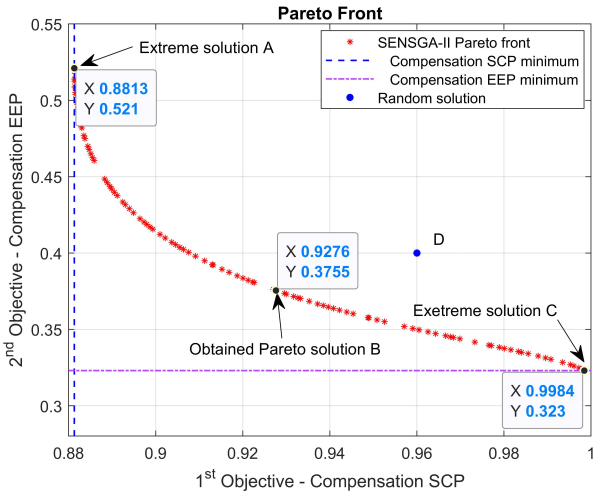

Figure 6. The Pareto front shows the optimal results for the two goals of (P2).

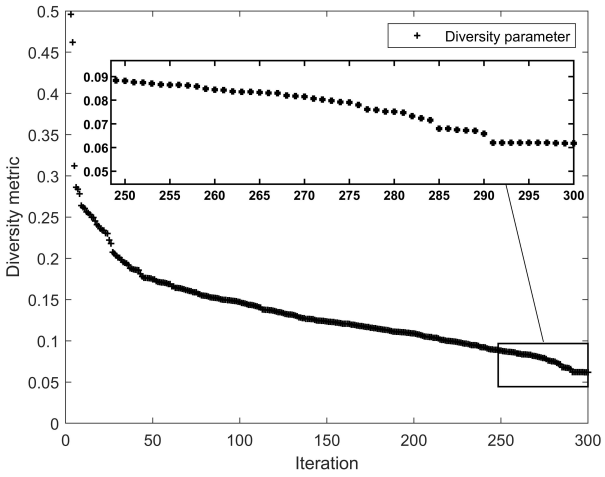

Figure 7. The convergence of SENSGA-II based on diversity metric.

0.323) in PF, to compare with the random one D(0.96, 0.4) taken in the feasible solution space. Obviously, solution A has minimum $\overline{\Phi_s}$ and maximum $\overline{\Psi_e}$, while solution C has maximum $\overline{\Phi_s}$ and minimum $\overline{\Psi_e}$. It means that there is no superior solution between these two solutions. Continuing, the solution pair B and also belongs to PF because the compensation SCP is better than C's, while the compensation EEP of C is better. Next, we compare solution D with C, and we observe that the second goal of solution C is better than D, but conversely, the first goal of solution D is better than C. Thus, if we do not use the PF, D would belong to the same ranking as solution C. However, our solution demonstrates the fact that solutions C and B are not dominant over each other, but solution D is dominated by B. Therefore, D is not optimal and is a dominant solution. The concept of the multi-objective optimal solution is confirmed as shown in the formula (19).

Another comment is that compensation SCP increases to 0.9984, then compensation EEP will decrease and reach a limit (value is 0.323) and cannot be reduced further. Meanwhile, when the compensation EEP increases to 0.8813, the compensation SCP will decrease and reach the limit value of 0.521. The results show that if the design option favors SCP optimization, then solution A should be chosen. If the option favors EEP optimality, solution C should be selected, or if the balance is between SCP and EEP, solution B should be chosen.

Finally, we investigate the convergence of SENSGA-II using the diversity metric in Fig. 7. Initially, a high value of $\mathcal{D}$ indicates that the solutions are not asymptotic to PF. Then the value $\mathcal{D}$ decreases if we continue increasing the maximum number of iterations. We see that the convergence trend slows down, showing that the solutions are distributed more and more uniformly. The subgraph depicting the diversity metric at loops 250 to 300 shows that over 50 evolutions, $\mathcal{D}$ only improved by approximately 0.03. In the last loops, $\mathcal{D}$ converged to 0.0621 and could not improve further. Although the $\mathcal{D}$ value has dropped to a deficient and acceptable level after the $MaxIt$ loop, the optimal value of 0 has not yet been reached. This also demonstrates in Fig. 6, when multiple spaces on the PF are not covered. It shows that the approaches to solving multi-objective optimization problems based on meta-heuristic such as SENSGA-II have high efficiency, but the obtained result is always at a near-optimal level. Furthermore, the dependence on initialization parameters based on a GA-based algorithm must be done in the next studies.

Remark 2. From Figs. 3-6, we can observe that the analysis and simulation results are matching very well. It means that the correctness of our analysis has been verified.

5. Conclusion

This paper has studied the system performance and optimization of IRS-assisted RF EH MEC NOMA networks under Nakagami-m fading. Specifically, we investigate the NOMA-MEC model for two edge-users who need to offload tasks to proximity HAP. An IRS element is deployed to the system to support the far-user operations. Accordingly, we propose a protocol for the system consisting of 4 phases, namely the energy harvesting phase, offloading phase, data processing phase, and result downloading phase. We evaluate system performance based on two parameters, SCP and EEP, and detect their trade-offs. Therefore, we state a multi-objective maximization problem for SCP and EEP with the constraint of time switching

ratio. We propose a low complexity algorithm, namely SENSGA-II, to determine the PF of the optimization problem. Next, we use the Monte-Carlo simulation to confirm the correctness of the theoretical analysis. The simulation results show that the system performance is highly dependent on parameters such as transmit power, time switching coefficient, task sequence length, and bandwidth. Furthermore, the PF obtained SENSGA-II indicates that extreme solutions and other optimal solutions are better than the solution of randomly choosing the α parameter.

In our future work, we will investigate the RF EH MEC NOMA system with multiple IRS assisting two users in energy harvesting and task offloading. We will apply other multi-objective optimization algorithms such as NSGA-III or MOPSO to reference the results obtained in this study.

Appendix A. Proof of Lemma 1

This appendix provides the detailed proof for Lemma 1. According to (14), we have:

$$\begin{aligned}\mathbf{\Phi_s} &= \Pr\left(\frac{L_1}{W\log_2(1+\gamma_1)}+(1-\alpha)\frac{\xi L}{f}<(1-\alpha)T_{th},\right.\\ &\qquad \left.\frac{L_2}{W\log_2(1+\gamma_2)}+(1-\alpha)\frac{\xi L}{f}<(1-\alpha)T_{th}\right)\\ &= \Pr\left(\gamma_1>2^{\frac{L_1}{WT^*}}-1,\gamma_2>2^{\frac{L_2}{WT^*}}-1\right)\\ &= \Pr\left(\frac{a\gamma_0\alpha_1X^2}{a\gamma_0\alpha_2Y^2+1}>\gamma_1^{th},a\gamma_0\alpha_2Y^2>\gamma_2^{th}\right)\\ &= \Pr\left(X>\sqrt{b_1Y^2+b_2},Y>\sqrt{b_0}\right)\\ &= \int_{\sqrt[4]{b_0}}^{\infty}\left[1-F_X\left(\sqrt{b_1z^4+b_2}\right)\right]f_Z(z)dz,\end{aligned}$$

where $L=L_1+L_2$, $T^*=(1-\alpha)\left[T_{th}-\frac{\xi L}{f}\right]$, $\gamma_1^{th}=2^{\frac{L_1}{WT^*}}-1$, $\gamma_2^{th}=2^{\frac{L_2}{WT^*}}-1$, $b_0=\frac{\gamma_2^{th}}{a\alpha_2\gamma_0}$, $b_1=\frac{\gamma_1^{th}\alpha_2}{\alpha_1}$, $b_2=\frac{\gamma_1^{th}}{a\gamma_0\alpha_1}$. Moreover, $F_X(x)$ is the CDF of $X=|h_1|^2$ follows the Nakagami-m fading model with fading parameter m_1. Thus, it is given by

$$F_X(x)=1-\sum_{k=0}^{m_1-1}\frac{m_1^kx^k}{k!\lambda_1^k}e^{-\frac{m_1x}{\lambda_1}}, \tag{A.1}$$

where $\lambda_1=\mathbb{E}\left[|h_1|^2\right]$, $\mathbb{E}[.]$ stands for the expectation operator. Note that it is NLoS for $m_1=1$ and is LoS for $m_1>1$.

Substituting (10) and (A.1) into Φ_s, we obtain

$$\begin{aligned}\mathbf{\Phi_s} &= \frac{m^N}{\Gamma(2m_sN)}\sum_{k=0}^{m_1-1}\frac{m_1^k}{k!\lambda_1^k}\int_{\sqrt[4]{b_0}}^{\infty}z^{2m_sN-1}\\ &\quad\times\left(b_1z^4+b_2\right)^{\frac{k}{2}}e^{-\frac{m_1}{\lambda_1}\sqrt{b_1z^4+b_2}-2\sqrt{m_sm_l}z}dz\\ &\overset{(1)}{=}\frac{m^N}{\Gamma(2m_sN)}\sum_{k=0}^{m_1-1}\frac{m_1^k}{k!\lambda_1^k}\int_0^{a_0}(-\ln t)^{2m_sN-1}\\ &\quad\times\left(b_1(-\ln t)^4+b_2\right)^{\frac{k}{2}}e^{-\frac{m_1}{\lambda_1}\sqrt{b_1(-\ln t)^4+b_2}}\\ &\quad\times\frac{e^{-2\sqrt{m_sm_l}(-\ln t)}}{t}dt\\ &\overset{(2)}{\approx}\frac{\pi a_0m^N}{2Q_1\Gamma(2m_sN)}\sum_{k=0}^{m_1-1}\sum_{q=1}^{Q_1}\frac{m_1^k}{k!\lambda_1^k}(-\ln t_q)^{2m_sN-1}\\ &\quad\times\left[b_1(-\ln t_q)^4+b_2\right]^{\frac{k}{2}}e^{-\frac{m_1}{\lambda_1}\sqrt{b_1(-\ln t_q)^4+b_2}}\\ &\quad\times\frac{e^{-2\sqrt{m_sm_l}(-\ln t_q)}}{t_q}\sqrt{1-x_q^2},\end{aligned}$$

where Step (1) is obtained by replacing $t=e^{-z}$ and $a_0=e^{-\sqrt[4]{b_0}}$. Step (2) is held by applying the Gaussian-Chebyshev quadrature method with Q_1 is the complexity-vs-accuracy trade-off coefficient, $x_q=\cos\left(\frac{2q-1}{2Q_1}\pi\right)$, $t_q=\frac{(x_q+1)a_0}{2}$. This concludes our proof.

Appendix B. Proof of Theorem 2

This appendix provides the detailed proof for Theorem 2. $\mathbf{\Psi_e}$ is calculated as follows:

$$\begin{aligned}\mathbf{\Psi_e} &= \Pr\left(\frac{P_0\alpha T}{\sum_{i=1}^{2}(1-\alpha)W\log_2(1+\gamma_i)}<\psi_{th}\right)\\ &= \Pr\left[(1+\gamma_1)(1+\gamma_2)>\gamma_{th}\right]\\ &= \Pr\left(a\gamma_0\alpha_1X^2>\gamma_{th}-a\gamma_0\alpha_2Y^2-1\right)\\ &= \int_0^{a_1}\left[1-F_X\left(\sqrt{c_1-c_2z^4}\right)\right]f_Z(z)dz+\int_{a_1}^{\infty}f_Z(z)dz\\ &= 1-F_Z(a_1)+\frac{m^N}{\Gamma(2m_sN)}\sum_{k=0}^{m_1-1}\frac{m_1^k}{k!\lambda_1^k}\int_0^{a_1}z^{2m_sN-1}\\ &\quad\times\left(c_1-c_2z^4\right)^{\frac{k}{2}}e^{-\frac{m_1}{\lambda_1}\sqrt{c_1-c_2z^4}-2\sqrt{m_sm_l}z}dz\\ &\overset{(3)}{\approx}1-F_Z(a_1)+\frac{\pi a_1m^N}{2Q_2\Gamma(2m_sN)}\sum_{k=0}^{m_1-1}\sum_{q=1}^{Q_2}\frac{m_1^k}{k!\lambda_1^k}\\ &\quad\times u_q^{2m_sN-1}\left[c_1-c_2u_q^4\right]^{\frac{k}{2}}e^{-\frac{m_1}{\lambda_1}\sqrt{c_1-c_2u_q^4}-2\sqrt{m_sm_l}u_q}\\ &\quad\times\sqrt{1-x_q^2},\end{aligned}$$

where $\gamma_{th}=2^{\frac{\alpha TP_0}{(1-\alpha)W\psi_{th}}}$, $c_1=\frac{\gamma_{th}-1}{a\gamma_0\alpha_1}$, $c_2=\frac{\alpha_2}{\alpha_1}$, $a_1=\sqrt[4]{\frac{c_1}{c_2}}$. Step (3) is derived by applying the Gaussian-Chebyshev quadrature method with Q_2 is the complexity-vs-accuracy trade-off coefficient, $x_q=\cos\left(\frac{2q-1}{2Q_2}\pi\right)$, $u_q=\frac{(x_q+1)a_1}{2}$. This ends our proof.

References

[1] Y. Mao, C. You, J. Zhang, K. Huang, and K. B. Letaief, "A survey on mobile edge computing: The communication perspective," *IEEE Communications Survey Tutorials*, vol. 19, no. 4, pp. 2322–2358, 2017.

[2] F. Zhou, Y. Wu, R. Q. Hu, and Y. Qian, "Computation rate maximization in uav-enabled wireless powered mobile-edge computing systems," *IEEE Journal on Selected Areas in Communications*, vol. 36, no. 9, pp. 1927–1941, 2018.

[3] H. Sun, F. Zhou, and R. Q. Hu, "Joint offloading and computation energy efficiency maximization in a mobile edge computing system," *IEEE Transactions on Vehicular Technology*, vol. 68, no. 3, pp. 3052–3056, 2019.

[4] Y. Zhang, X. Lan, Y. Li, L. Cai, and J. Pan, "Efficient computation resource management in mobile edge-cloud computing," *IEEE Internet of Things Journal*, vol. 6, no. 2, pp. 3455–3466, 2019.

[5] D. Van Huynh, S. R. Khosravirad, A. Masaracchia, O. A. Dobre, and T. Q. Duong, "Edge intelligence-based ultra-reliable and low-latency communications for digital twin-enabled metaverse," *IEEE Wireless Communications Letters*, pp. 1–1, 2022.

[6] T. X. Tran and D. Pompili, "Joint task offloading and resource allocation for multi-server mobile-edge computing networks," *IEEE Transactions on Vehicular Technology*, vol. 68, no. 1, pp. 856–868, 2018.

[7] X. Zhou, R. Zhang, and C. Ho, "Wireless information and power transfer: architecture design and rate-energy tradeoff," *IEEE Trans. Commun.*, vol. 61, no. 11, pp. 4757–4767, Nov. 2013.

[8] D.-B. Ha and Q. S. Nguyen, "Outage performance of energy harvesting DF relaying NOMA networks," *Mobile Networks and Applications*, 2017.

[9] D.-B. Ha, D.-D. Tran, T.-V. Truong, and N.-V. Vo, "Physical layer secrecy performance of energy harvesting networks with power transfer station selection," in *IEEE International Conference on Communications and Electronics (ICCE)*, 2016, pp. 451–456.

[10] A. A. Nasir, X. Zhou, S. Durrani, and R. A. Kennedy, "Relaying protocols for wireless energy harvesting and information processing," *IEEE Transactions on Wireless Communications*, vol. 12(7), pp. 3622–3636, 2013.

[11] D.-B. Ha, V.-T. Truong, and Y. Lee, "Performance analysis for RF energy harvesting mobile edge computing networks with SIMO/MISO-NOMA schemes," *EAI Endorsed Transactions on Industrial Networks and Intelligent Systems*, vol. 8, no. 27, pp. 1–14, Apr. 2021.

[12] V.-T. Truong, D.-B. Ha, T.-V. Truong, and A. Nayyar, "Performance analysis of rf energy harvesting noma mobile edge computing in multiple devices iiot networks," in *International Conference on Industrial Networks and Intelligent Systems*. Springer, 2022, pp. 62–76.

[13] D. H. Ha, D.-B. Ha, V.-T. Truong, V.-D. Phan, and Q. S. Vu, "Performance enhancement of wireless sensor network by using non-orthogonal multiple access and sensor node selection schemes," *Indonesian Journal of Electrical Engineering and Computer Science*, vol. 21, no. 2, pp. 886–894, Feb. 2021.

[14] F. Zhou, Y. Wu, R. Q. Hu, and Y. Qian, "Computation efficiency in a wireless-powered mobile edge computing network with NOMA," in *IEEE International Conference on Communications (ICC), Shanghai, China, 20-24 May 2019*, 2019.

[15] Y. Ye, G. Lu, R. Q. Hu, and L. Shi, "On the performance and optimization for MEC networks using uplink NOMA," in *IEEE International Conference on Communications Workshops (ICC Workshops), Shanghai, China*. IEEE, 2019.

[16] V.-T. Truong, D.-B. Ha, V. N. Vo, and C. So-In, "On the system performance of mobile edge computing in an uplink NOMA WSN with a multi-antenna access point over nakagami-m fading," *IEEE/CAA Journal of Automatica Sinica*, vol. 9, no. 4, pp. 253–264, Apr. 2022.

[17] L. Dai, B. Wang, M. Wang, X. Yang, J. Tan, S. Bi, S. Xu, F. Yang, Z. Chen, M. D. Renzo, C.-B. Chae, and L. Hanzo, "Reconfigurable intelligent surface-based wireless communications: Antenna design, prototyping, and experimental results," *IEEE Access*, vol. 8, pp. 45 913–45 923, 2020.

[18] R. Alghamdi, "Intelligent surfaces for 6g wireless networks: A survey of optimization and performance analysis techniques," *IEEE Access*, vol. 8, pp. 202 795–202 818, 2020.

[19] Z. Chen, X. Ma, C. Han, and Q. Wen, "Towards intelligent reflecting surface empowered 6g terahertz communications: A survey," *China Communications*, vol. 18, no. 5, pp. 93–119, 5 2021.

[20] T. Bai, C. Pan, Y. Deng, M. Elkashlan, A. Nallanathan, and L. Hanzo, "Latency minimization for intelligent reflecting surface aided mobile edge computing," *IEEE Journal on Selected Areas in Communications*, vol. 38, pp. 2666–2682, 2020.

[21] G. Yang, X. Xu, and Y. Liang, "Intelligent reflecting surface assisted non-orthogonal multiple access," in *2020 IEEE Wireless Communications and Networking Conference (WCNC)*, 2020, pp. 1–6.

[22] Z. Chu, P. Xiao, M. Shojafar, D. Mi, J. Mao, and W. Hao, "Intelligent reflecting surface assisted mobile edge computing for internet of things," *IEEE Wireless Communications Letters*, vol. 10, no. 3, pp. 619–623, 3 2021.

[23] Y. Cheng, K. H. Li, Y. Liu, K. C. Teh, and H. Vincent Poor, "Downlink and uplink intelligent reflecting surface aided networks: NOMA and OMA," *IEEE Transactions on Wireless Communications*, vol. 20, no. 6, 2021. [Online]. Available: http://dx.doi.org/10.1109/TWC.2021.3054841

[24] M.-H. T. Nguyen, E. Garcia-Palacios, T. Do-Duy, O. A. Dobre, and T. Q. Duong, "Uav-aided aerial reconfigurable intelligent surface communications with massive mimo system," *IEEE Transactions on Cognitive Communications and Networking*, pp. 1–13, 2022.

[25] F. Zhou, C. You, and R. Zhang, *Delay-Optimal Scheduling for IRS-Aided Mobile Edge Computing*, 4 2021, vol. 10, no. 4, pp. 740–744.

[26] G. Chen, Q. Wu, W. Chen, D. W. K. Ng, and L. Hanzo, "IRS-aided wireless powered MEC systems: TDMA or NOMA for computation offloading?" 2021.

[27] D.-B. Ha, V.-T. Truong, and V. N. Vo, "Performance analysis of intelligent reflecting surface-aided mobile edge computing network with uplink NOMA scheme," *International Conference on Industrial Networks and Intelligent Systems (INISCOM)*, Apr. 2022.

[28] D.-B. Ha, D.-D. Tran, V. Tran-Ha, and E.-K. Hong, "Performance of amplify-and-forward relaying with wireless power transfer over dissimilar channels," *Elektronika ir Elektrotechnika Journal*, vol. 21, no. 5, pp. 90–95, 2015.

[29] C. Huang, A. Zappone, G. Alexandropoulos, M. Debbah, and C. Yuen, "Reconfigurable intelligent surfaces for energy efficiency in wireless communications," *IEEE Transactions on Wireless Communications*, vol. 18, no. 8, pp. 4157–4170, Aug. 2019.

[30] S. Mao, S. Leng, S. Maharjan, and Y. Zhang, "Energy efficiency and delay tradeoff for wireless powered mobile-edge computing systems with multi-access schemes," *IEEE Transactions on Wireless Communications*, vol. 19, no. 3, pp. 1855–1867, Mar. 2020.

[31] S. Dutta and K. N. Das, "A survey on pareto-based eas to solve multi-objective optimization problems," *Soft Computing for Problem Solving*, pp. 807–820, 2019.

[32] K. Deb, A. Pratap, S. Agarwal, and T. Meyarivan, "A fast and elitist multiobjective genetic algorithm: Nsga-ii," *IEEE transactions on evolutionary computation*, vol. 6, no. 2, pp. 182–197, 2002.

[33] M. Srinivas and L. M. Patnaik, "Genetic algorithms: A survey," *computer*, vol. 27, no. 6, pp. 17–26, 1994.

[34] F.-A. Fortin and M. Parizeau, "Revisiting the nsga-ii crowding-distance computation," in *Proceedings of the 15th annual conference on Genetic and evolutionary computation*, 2013, pp. 623–630.

[35] P. Kora and P. Yadlapalli, "Crossover operators in genetic algorithms: A review," *International Journal of Computer Applications*, vol. 162, no. 10, 2017.

[36] G. Chen, Q. Wu, W. Chen, D. W. K. Ng, and L. Hanzo, "Irs-aided wireless powered mec systems: Tdma or noma for computation offloading?" *arXiv preprint arXiv:2108.06120*, 2021.

Dac-Binh Ha received the B.S. degree in Radio Technique, the M.Sc. and Ph.D. degree in Communication and Information System from Huazhong University of Science and Technology (HUST), China in 1997, 2006, and 2009, respectively. He is currently the Dean of School of Engineering and Technology, Duy Tan University, Da Nang, Vietnam. His research interests are B5G/6G networks, mobile edge computing, quantum computing and communications. He has published several papers on ISI/SCI/SCIE index journals, such as IEICE Transactions, Journal of Communications and Network, Wireless Communications and Mobile Computing, IETE Journal of Research, Elektronika ir Elektrotechnika, Wireless Personal Communications, IET Communications, Mobile Networks and Applications, Sensors, IEEE Access, IEEE System and IEEE/CAA Journal of Automatica Sinica.

Van-Truong Truong received a B.S. degree in Electronics and Telecommunication Engineering and an M.Sc. in Electronic Engineering from the University of Da Nang, Vietnam. He is currently a Ph.D. student and Dean of the Faculty of Electrical and Electronics Engineering, Duy Tan University, Da Nang, Vietnam. His research interests include non-orthogonal multiple access, wireless sensor networks, mobile edge computing and the IoT. He has published several papers on ISI index journals, such as IEEE/CAA Journal of Automatica Sinica, Mobile Networks and Applications, IEEE Access, Computers Materials & Continua, and PeerJ Computer Science.

Yoonill Lee is currently a faculty of Electrical Engineering Technology at the College of Lake County, Grayslake, IL. He earned his B.S. and M.S. in Electrical Engineering from Yonsei University in Seoul, South Korea, in 1984, 1986, respectively, and M.S. in Electrical Engineering from Oklahoma State University in Stillwater, OK in 1992, and Ph.D. in Electrical Engineering from the University of South Florida in Tampa, FL in 2001. He worked at Cisco Systems as a communications engineer. His research interests include CDMA, Multi-Carrier Systems, MIMO Technology, and Physical Layer Security in Wireless Communication Systems. He has published several papers for IEEE and holds a U.S. patent.